Composites based on heparin and MIL-101(Fe)

The drug releasing depot for anticoagulant therapy and advanced medical nanofabrication

Vinogradov, Vladimir V.; Drozdov, Andrey S.; Mingabudinova, Leila R.; Shabanova, Emiliya M.; Kolchina, Nina O.; Anastasova, Elizaveta I.; Markova, Alina A.; Shtil, Alexander A.; Milichko, Valentin A.; Starova, Galina L.

DOI
10.1039/c8tb00072g

Publication date
2018

Document Version
Final published version

Published in
Journal of Materials Chemistry B

Journal of Materials Chemistry B

PAPER

View Article Online
View Journal | View Issue

Cite this: J. Mater. Chem. B, 2018, 6, 2450

Composites based on heparin and MIL-101(Fe): the drug releasing depot for anticoagulant therapy and advanced medical nanofabrication†

Vladimir V. Vinogradov,*[a] Andrey S. Drozdov,[a] Leila R. Mingabudinova,[a] Emiliya M. Shabanova,[a] Nina O. Kolchina,[a] Elizaveta I. Anastasova,[a] Alina A. Markova,[b] Alexander A. Shtil,[ac] Valentin A. Milichko,[d] Galina L. Starova,[e] Rafaella L. M. Precker,[f] Alexandr V. Vinogradov,[a] Evamarie Hey-Hawkins[f] and Evgeny A. Pidko*[ag]

Received 9th January 2018,
Accepted 21st February 2018

DOI: 10.1039/c8tb00072g

rsc.li/materials-b

We describe the synthesis and properties of a new composite material based on heparin and MIL-101(Fe) metal–organic framework. The intrinsic instability of MIL-101(Fe) towards hydrolysis enables binding of heparin molecules to the framework structure as is evidenced by DFT calculations and adsorption experiments. The *de novo* formed heparin–MOF composites showed good biocompatibility in *in vitro* and demonstrated pronounced anticoagulant activity. The specific interaction between the bioactive molecule and the carrier is critical for the selective degradation of the complex in the body fluids and for the enhanced activity. Hep_MIL-101(Fe) composite could serve as a drug-releasing depot for nanofabrication and to introduce anticoagulant activity to medical devices and biocoatings. Addition of Hep_MIL-101(Fe) to a sol–gel derived thrombolytic matrix allowed the combination of anticoagulant and thrombolytic activities in a single hybrid nanomaterial that could be applied as a bioactive nanocoating for PTFE vein implants.

1 Introduction

Development of smart drugs with a targeted and controllable mechanism of action is a rapidly growing field at the interface of chemistry, material sciences and biomedicine.[1–4] Next to the search for new bioactive molecules and functional drugs with a higher efficacy and attenuated side effects, engineering of encapsulation matrices and targeted delivery systems is an important strategy towards the new generations of innovative pharmaceuticals. Of particular interest are the chemical systems in which drug release can be triggered in response to external stimuli (*e.g.*, inflammation, changes of glucose concentration, acidification of the peritumoral milieu, *etc.*).[1,5–9] This approach not only provides a mechanism for targeted drug delivery but also helps to control the drug dosage in the body triggered by external stimuli. The development of pharmaceutical systems with a self-regulating adjustment is often considered one of the key challenges in the field.[10,11] In recent years, there has been a growing interest in the biomedical applicability of hybrid materials such as metal–organic frameworks (MOFs) combining the properties of both organic and inorganic systems.[12–15] A major advantage of these materials for the controlled drug release over the conventional supramolecular and polymer-based matrices is a high tunability of their structure-forming inorganic joints. This property makes MOFs responsive to particular stimuli. This property may be utilized to engineer MOFs responsive to specific external stimuli. By selecting an appropriate metal–ligand combination, the specific re-structuring of the hybrid matrix can be achieved.[12,16–20] The possibility to select specific pore topologies of the MOF material, the presence of functional groups on the organic ligands and the accessibility together with the tailored chemical reactivity of the metal sites allow the properties of the final material to be optimized for targeted delivery of biomolecules. Drug encapsulation and release can be further facilitated by MOF swelling, breathing behavior, flexibility

[a] Laboratory of Solution Chemistry of Advanced Materials and Technologies, ITMO University, Lomonosova st. 9, Saint-Petersburg, 197101, Russian Federation. E-mail: e.a.pidko@tudelft.nl, vinogradov@scamt-itmo.ru
[b] A.N.Nesmeyanov Institute of Organoelement Compounds, Russian Academy of Sciences, Vavilova st., 28, Moscow, 119991, Russian Federation
[c] Blokhin National Medical Research Center of Oncology, 24 Kashirskoye shosse, Moscow 115478, Russian Federation
[d] Department of Nanophotonics and Metamaterials, ITMO University, Birjevaya st. 14, Saint-Petersburg, 192001, Russian Federation
[e] Department of Chemistry, Saint-Petersburg State University, Universitetskaya st. 26, Saint-Petersburg, 198504, Russian Federation
[f] Institute of Inorganic Chemistry, Leipzig University, Johannisallee 19, Leipzig, D-04103, Germany
[g] Inorganic Systems Engineering group, Department of Chemical Engineering, Delft University of Technology, Van der Maasweg 9, Delft, 2629 HZ, The Netherlands

† Electronic supplementary information (ESI) available. See DOI: 10.1039/c8tb00072g

with thermal expansion or compression triggered by interactions with guest molecules, linker rotation, subnetwork displacements, *etc.*[21–28]

For practical applications, a drug delivery system based on the response-engineered MOF matrices would require the use of a combination of functional materials. In particular, encapsulation of a MOF material into FDA-approved sol–gel matrices represents a promising approach for avoiding direct contact with the blood and improving the mechanical properties of the nanostructured hybrid material. The sol–gel technology is particularly advantageous due to its chemical simplicity, easy scale-up and a high biocompatibility. Previous studies demonstrated a high potential of sol–gel methodologies for fabrication of magnetic drug delivery systems,[29–32] proteolytic sol–gel materials for non-invasive surgery,[33] as well as durable coatings with a high thrombolytic activity.[34–37] In this study, we combined the approaches of drug encapsulation within the responsive MOF matrix with sol–gel thrombolytic materials to develop a new hybrid strategy of anticoagulant treatment. We took advantage of the biocompatible MIL-101(Fe) MOF as the heparin drug carrier and combined it with a ceramic thrombolytic sol–gel coating in order to create the hybrid material with an extended profile of action. For this purpose, heparin molecules (Fig. 1a) were complexed with the MOF material (Fig. 1b) and the heparin–MIL-101 hybrid (Hep_MIL-101) was co-entrapped with streptokinase within the inorganic sol–gel matrix. The synthetic strategy for preparation of this four-component biocomposite coating is illustrated in Fig. 1c. Our study reveals an enhanced anticoagulant activity of the composite matrix associated with the release of the Hep_MIL-101(Fe) degradation product rather than with the direct desorption of the original polysaccharide. Based on the results of density functional theory (DFT) calculations, we propose a mechanism of molecular interactions in this complex and their role in drug release and enhanced therapeutic efficacy.

2 Results and discussion

2.1 Heparin–MOF composites

First, we investigated the role of lattice stability and the adsorption capacities of the biocompatible MIL-101(Fe). The properties of MIL-101(Fe) were compared with those derived for the model system based on the chromium-based counterpart MIL-101(Cr). Despite the similarity of the crystal structures, the stability of the two frameworks differed dramatically. Whereas the Cr-based framework showed an outstanding stability that allows the broad applicability of this material as a catalyst support,[38–40] the intrinsic instability of MIL-101(Fe) towards hydrolysis results in an easier metabolism and therefore a higher biocompatibility. This different chemical behavior directly originates from the reactivity of the inorganic joints and can also be

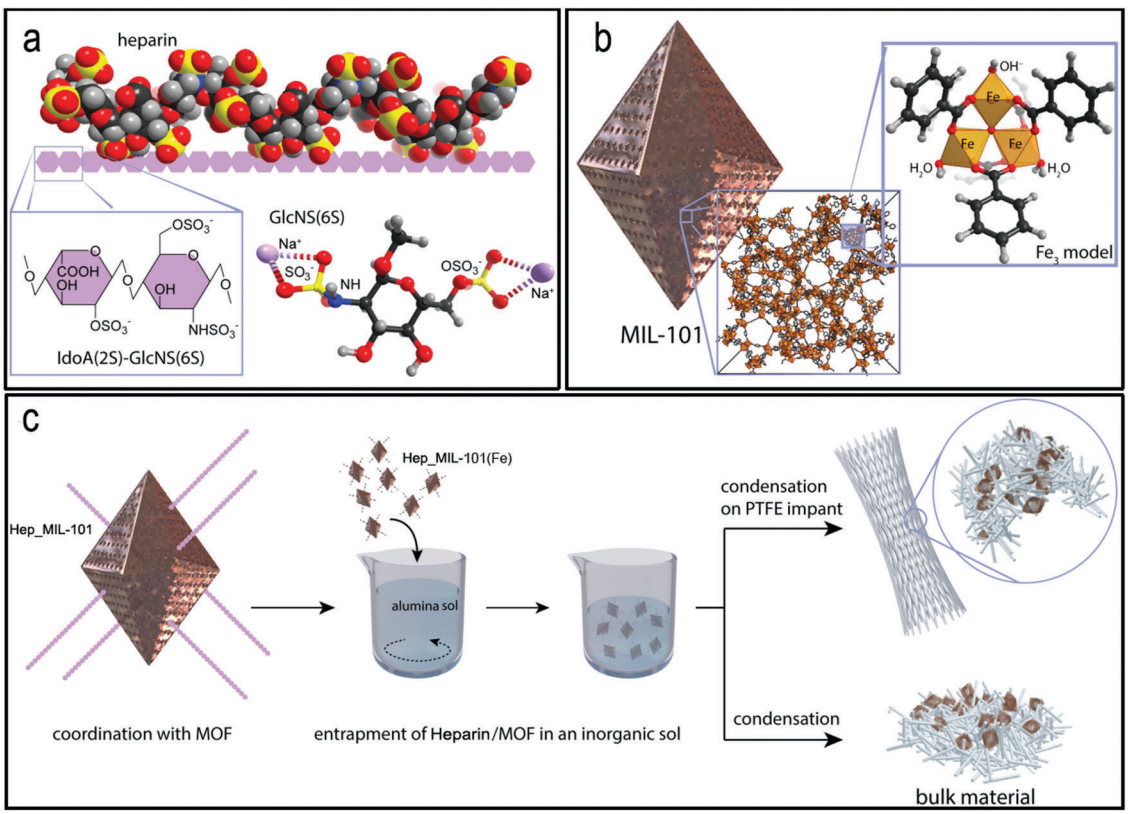

Fig. 1 Complexation of (a) heparin with (b) metal sites of the MIL-101(Fe) MOF yields a biocomposite for (c) thrombolytic coating with prolonged anticoagulant activity (enzymes and Hep_MIL-101 entrapped in a sol–gel matrix).

Table 1 Hydrodynamic parameters of MOF NPs and heparin–MOF composites

	Medium	MIL-101(Fe)	Hep_MIL-101(Fe)
BET surface area ($m^2\ g^{-1}$)		1700	1452
Size (nm)	Water	151	163
	PBS	143	168
	Plasma	164	142
Zeta-potential (mV)	Water	+23	−27
	PBS	+14	−35
	Plasma	−15	−29

manifested in the adsorption and drug-delivery characteristics of the two materials. Heparin adsorption on MIL-101 nanoparticles (NP) was studied by incubating the MOF samples in heparin water solution followed by centrifugation and washing with water to remove excess physisorbed heparin (see Experimental for details). The amount of adsorbed heparin was determined spectrophotometrically and by a thermogravimetric analysis. For MIL-101(Fe), a fast and efficient adsorption of heparin was observed. Already after 5 min of incubation, 90% of the polysaccharide was immobilized on the solid, evidencing a fast grafting kinetics and a high affinity of heparin to the surface of MIL-101(Fe). The profile of Hep_MIL-101(Fe) release in distilled water demonstrated that the adsorption is irreversible (see the ESI,† Fig. S1). The loading capacity of MIL-101(Fe) was determined as 15 wt% of heparin with respect to the dry MOF. This can be translated into 1500 IU g^{-1} of heparin activity for the Hep_MIL-101(Fe) composite (see the ESI,† Fig. S2). Dynamic light scattering and nitrogen physisorption (Table 1) characterization of the material before and after adsorption of heparin showed changes in surface properties indicative of the formation of adsorption complexes on the MOF surface. In particular, adsorption of heparin on the surface of MIL-101(Fe) led to an insignificant increase of the hydrodynamic diameter of particles of an average of 12 nm (from 151 nm to 163 nm) (Table 1). The increase of the particle size corresponds to the sorption of the heparin layer on the surface of the particles. Sorption of a highly charged polyelectrolyte significantly changed the surface charge of the MOF NPs and shifted it to a more negative value. MIL-101(Fe) is positively charged in an aqueous medium with a value of +23 mV, while adsorption of heparin confers the opposite charge (−27 mV). In physiological media such as phosphate buffered saline (PBS) and blood plasma, the negative charge of the Hep_MIL-101(Fe) surface increased to the values −35 mV and −29 mV, respectively. These high values of negative charge ensure the stability of the resulting colloidal solutions of this composite due to electrostatic repulsion. Next, we employed the Ga^+ etching technique in combination with electron microscopy and EDS mapping to probe the chemical composition of the biocomposite and estimate the depth of heparin penetration into the MOF crystallites. Representative SEM images with EDS mappings of Fe and S of the crystallite surface before and after Ga etching are shown in Fig. 2. The external surface of the Hep_MIL-101(Fe) crystallite (Fig. 2(a–c)) is completely covered with heparin as judged by a homogeneous distribution of iron associated with the MOF lattice and sulfur due to the adsorbed heparin. After etching, the elemental distribution changed substantially (Fig. 2(d–f)). The drop in the O-Kα1 and Fe-Kα1 signals is associated with the "shadow side" relative to the detector. These changes did not coincide with the S-Kα1 signal, providing evidence for the predominance of heparin at the surface and the absence of the respective EDS signal deeper inside the crystallites. This observation is in line with the fact that because of the much larger size of heparin polysaccharide compared to the aperture of the MOF nanopores, drug diffusion inside the pores is very unlikely. Adsorption is expected to occur only in the vicinity of the external surface. Heparin adsorption to the structurally much more stable MIL-101(Cr) was significantly less efficient compared to MIL-101(Fe). The maximum sorption capacity was below 2 wt%. Furthermore, unlike its Fe-based counterpart, MIL-101(Cr) adsorbs heparin reversibly and apparently forms no strong surface complexes. Otherwise, heparin release would be observed upon solvent replacement. We suggest that this difference in adsorption behavior is indicative of the intrinsically different mode of interaction between heparin and the structure-forming units of the MOF materials.

2.2 Interaction between heparin and MIL-101(Fe) determined by DFT

To get further insight into the nature of the heparin–MOF interaction and to understand the different adsorption behavior of the chromium and iron-based MIL-101 MOF materials, model density functional theory calculations (PBE-D3/6-311+G(d,p)//PBE-D3/6-31G(d)) were carried out. Here, we were particularly interested in understanding the local chemical interaction between the anionic moieties of the polysaccharide and individual transition metal-based nodes of the MOF structure. These phenomena were investigated by using local models of the two components, namely, the Glc(NS(6S)) monomer of heparin (Fig. 1(a)) and the Fe_3 cluster model representing the local structure of MIL-101 (Fig. 1(b)). Although such a cluster modeling approach does not account for long-range interactions and cooperative effects associated with the simultaneous binding on numerous sites on both components, these models are suitable for a semi-quantitative analysis of the local chemistry of the structure-forming units of the MOF.[41] A high-spin configuration of the tri-nuclear Fe_3O core has been assumed in all calculations. Preliminary calculations pointed to this electronic configuration as the preferred one for the current MOF model. A number of hypothetical structures representing different adsorption complexes of heparin with the Fe-MIL-101 cluster formed *via* the exchange of the H_2O ligand with the neutral electronegative groups or the condensation with the OH ligand, or the intrusion into the MOF structure. The most stable configurations were formed only for the H_2O exchange and the intrusion mechanism. Below, we focus on the analysis of the three most stable configurations and the energetics of their formation upon the interaction of the MIL-101 and heparin models (Fig. 3).

DFT calculations confirm the above discussion and reveal a high exothermicity of the reaction of heparin with the structure-forming trinuclear Fe_3O–carboxylate moieties resulting in rather stable surface adducts (Fig. 3a). The reaction of heparin with the MOF starts with the exchange of the weakly bound H_2O molecule

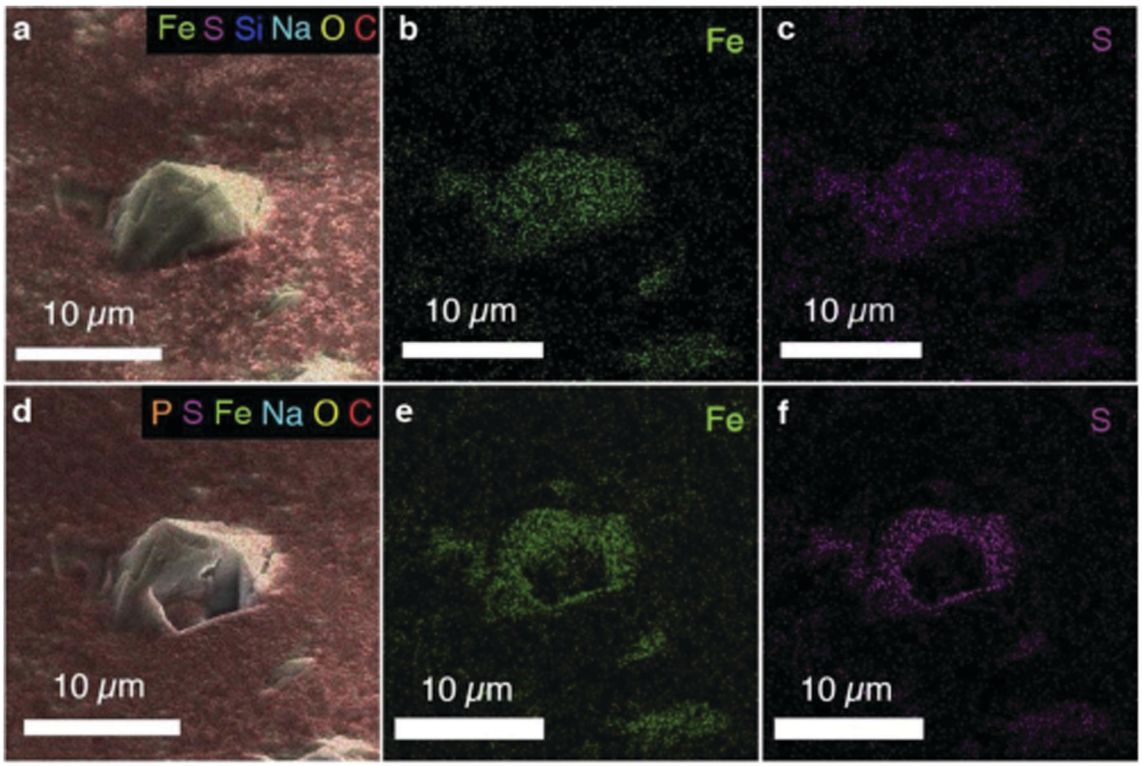

Fig. 2 SEM images with multilayer EDS-mapping of Hep_MIL-101(Fe). A Hep_MIL-101 crystal with edges on the surface (a); EDX-mapping of iron (b) and sulfur (c) on the crystal before etching; image of the Hep_MIL-101 crystal with lamellae produced by the focused Ga^+ ion beam etching method (d); EDX-mapping of iron (e) and sulfur (f) after etching.

at the Fe site with a neutral electronegative moiety of the heparin model ($Na^+Hep^{-}\cdots[Fe_3]$, Fig. 3b). The most favorable adsorption mode of this type is realized upon the coordination of the O_4–H hydroxyl to the open iron site. The anionic moieties are not involved in the coordination in this case. Even though such a ligand exchange-type adsorption is strongly exothermic (-102 kJ mol^{-1}), it affects only slightly the structure of the MOF model and does not alter the coordination environment of the Fe centers. This structure is a precursor for further reaction of the heparin with the Fe–carboxylate moieties that can be viewed as effectively an

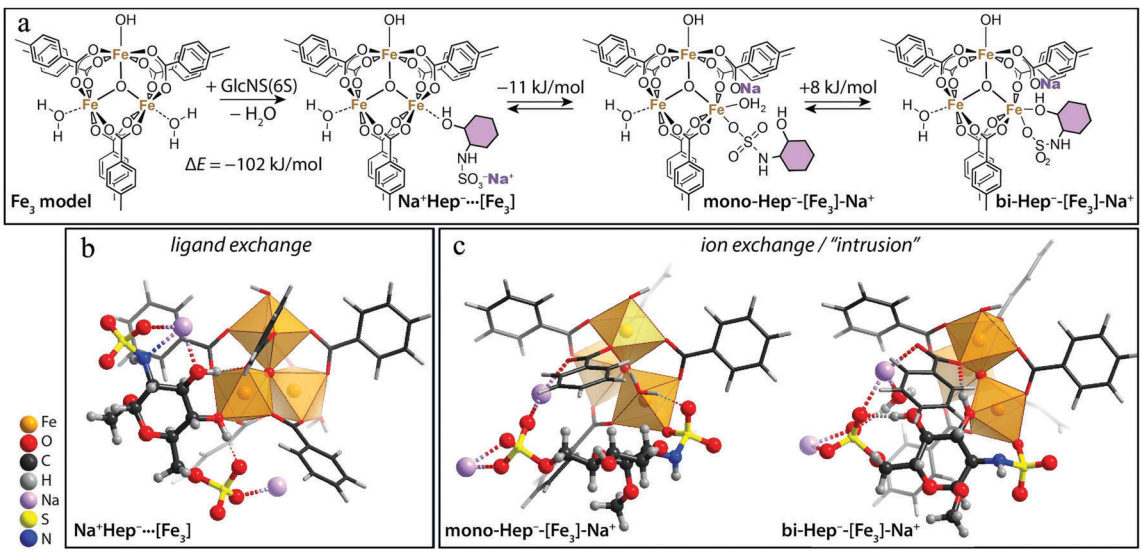

Fig. 3 (a) The most favorable path for the reaction and the DFT computed energetics for the elementary steps involved in the interaction of a heparin model with the trinuclear Fe-oxo node of the MIL-101 structure. Optimized structures of the GlcNS(6S)–Fe_3 complexes formed (b) at the initial ligand exchange step and (c) products of the subsequent intrusion of the anionic heparin into the MOF structure.

ion-exchange process between the heparin-Na salt and the Fe–terephthalate moiety (Fig. 3c) resulting in mono-Hep$^{-}\cdots$[Fe_3]-Na^+ that potentially can isomerize into a bidentate complex bi-Hep$^{-}\cdots$[Fe_3]-Na^+ by substituting the Fe-bound H_2O molecule. Such an intrusion of a drug molecule into the MOF lattice is predicted to be slightly exothermic and it results in a direct coordination of the anionic moiety of heparin, and the sodium cation forms a direct coordination bond with the carboxylate moiety of the MOF ligand. This adsorption mode results in a partial structural degradation of the trinuclear Fe_3O core. We propose that the more open coordination environment in the resulting structure makes it more susceptible to hydrolysis.

DFT predicts very close intrinsic stabilities of these different adsorption modes suggesting that all of them can potentially be realized on the MOF surface. The analysis of the computational results reveals that the stability of the adsorption complexes is provided by different types of interactions including weak van der Waals bonding between the π-systems of MOF ligands and the hydrophobic part of the glycoside moieties. The direct coordination between the chelating part of heparin and the iron cluster is critical. Taking into account the high value of binding constant between heparin and its natural substrate antithrombin-III (2×10^{-8} M) and significant enthalpy of interaction (−47 kJ mol^{-1}),[42] it could be speculated that in the course of competitive interaction, heparin could unbind from the surface of the Hep_MIL-101(Fe) composite to form a Hep–ATIII complex, realizing its bioactivity. Importantly, when the formation of similar adsorption complexes over a related [Cr_3] model is considered, even the first ligand exchange step is found to be quite unfavorable, showing reaction energies of over 30 kJ mol^{-1} according to DFT calculations. This suggests that heparin adsorption on the structurally much more stable MIL-101(Cr) material is limited to physisorption onto the organic walls dominated by very weak van der Waals forces. This is in agreement with the experimental data evidencing the very low adsorption capacity of this model material.

2.3 Anticoagulant activity of composite materials

Calculations reveal that the intrinsic structural instability of the MIL-101(Fe) material to hydrolysis is critical for the formation of a stable surface complex of bioactive molecules and the carrier. At the same time, this property is important for bioactivity. Indeed, degradation of the drug–carrier complex is expected to provide anticoagulant activity in the presence of antithrombin-III (ATIII). Thus, partial degradation of MIL-101(Fe) upon heparin adsorption may be viewed as advantageous when targeting a biodegradable heparin-releasing composite.

The anticoagulant activities of Hep_MIL-101(Fe) and Hep_MIL-101(Cr) were evaluated by monitoring the kinetic curves of coagulation of standard human plasma by measuring activated partial thromboplastin time (aPTT) (Fig. 4). The anticoagulant activity of the Hep_MIL-101(Fe) composite was almost as high as that of free heparin (aPTT value > 300 s). In contrast, the activity of Hep_MIL-101(Cr) was close to the reference value (aPTT 45 s for Hep_MIL-101(Cr) and 35 s for control plasma). Similar results were obtained by measuring prothrombin time

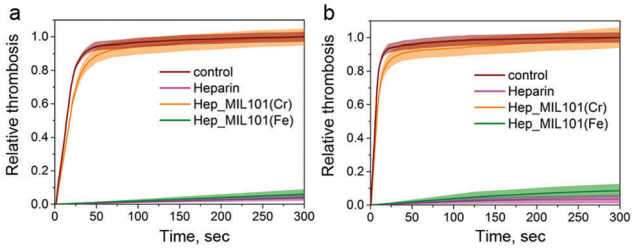

Fig. 4 Anticoagulant activity of Hep_MIL-101(Fe) and Hep_MIL-101(Cr) measured by aPTT assay (a) and pTT assay (b).

(pTT), which is clot formation. Both free heparin and Hep_MIL-101(Fe) inhibited coagulation by deactivating thrombin *via* its complexation with heparin. In contrast, in the presence of Hep_MIL-101(Cr), the prothrombin time (20 s) was close to the value of the control plasma (17 s). These data demonstrated an important feature of the Hep_MIL-101(Fe) composite. Indeed, direct coordination of the polysaccharide with the Fe sites involves the formation of bonds strong enough in water solution without heparin leakage, but after immersing in the blood plasma, degradation of the MOF structure results in the release of heparin and realizing the anticoagulant activity.

2.4 Cytotoxicity for cultured tumor cells

High drug loading capacity and effective anticoagulant activity of Hep_MIL-101(Fe) makes this material a good candidate to be used as a smart drug delivery biocomposite for anticoagulant therapy. The effectiveness of a drug is determined not only by therapeutic dose but also by its potential toxic effects. To investigate the prepared composites for their potential toxic effects, we evaluated the cytotoxicity of the materials *in vitro* on human colon cancer cell line HCT116. The HCT116 line does not differentiate or express CDX1, nor does it contain subpopulations of cells with greater tumor-forming capacity and it is often used for cytotoxicity testing of nano-objects.[43–45] Moreover, this cell line is heparin-sensitive due to proliferation modulation through p38 nitrogen-activated protein kinase signaling.[46] Cells were incubated for 72 hours at 37 °C, 5% CO_2, in a humidified atmosphere. 1 hour before the end of the incubation, 20 μL of an aqueous solution of MTT (5 mg mL^{-1}, PanEco, Russia) was added to the wells. After incubation, the culture medium was selected, the cells resuspended in 100 μL of DMSO, and the optical density of the solution was measured on a Multiscan FC (Thermo Scientific, USA) plate spectrophotometer at a wavelength of 570 nm. The percentage of cells that survived the action of each dose of the compound was counted as a quotient of the mean optical density in the wells after incubation with this dose to the average optical density of the control wells (the values of the latter were taken as 100%).

The results of the toxicity tests are summarized in Fig. 5. These data provide clear evidence of the non-toxic nature of the Hep_MIL-101 composites in a wide range of concentrations. While both iron and chrome ions are known to be cytotoxic due to involvement in reactive oxygen species formation processes, it was demonstrated previously that MIL-101 is stable at

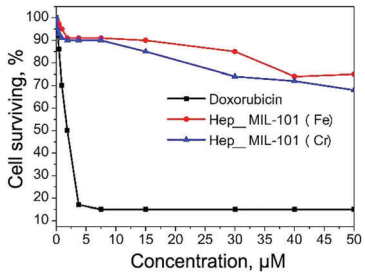

Fig. 5 The survival curve of HCT116 cells under the action of the control compound (doxorubicin) and under the action of suspension of Hep_MIL-101(Cr) and Hep_MIL-101(Fe).

temperatures lower than 60 °C and no metal ion leaching occurring under the used experimental conditions.[47,48] The cytotoxicity data also prove the DFT calculation results, demonstrating that upon interaction with heparin molecules, only partial discoordination of iron atoms from the crystal lattice is occurring, but the structure of MIL-101(Fe) remains mainly unchanged. The results obtained suggest that Hep_MIL-101 hybrids could be used for parenteral administration as individual heparin-releasing agents or as a component of nanocomposite materials providing an anticoagulant contribution to the overall bioactivity.

2.5 A hybrid sol–gel nanocoating with the anticoagulant Hep_MIL-101(Fe) composite

One of the possible application scenarios for the described materials is their application as a drug-releasing depot for application in thrombolytic coatings. Thrombolytic coatings for vascular implants or stents are recently developed ways to extend functional properties of implantable objects.[34–36,49] Such coatings consist of sol–gel derived biocompatible materials that are approved for parenteral administration (such as alumina or magnetite) with an immobilized thrombolytic enzyme that demonstrates a prolonged thrombolytic effect. While the long-lasting bioactivity of thrombolytic coatings is determined by their nanostructure and organization of the material, there is a risk of premature surface clogging due to rapid blood coagulation and potential blocking of nanopores of the coating. By using anticoagulants, such precocious inactivation of the coatings could be prevented. However, the direct entrapment of heparin or other anticoagulant agents into a sol–gel matrix is hindered by the specific features of the entrapment process and fast leakage of smaller (<5 nm) agents.[50] Thus, the anticoagulants should be used together with a carrying agent in order to provide the optimal biological effect, and Hep_MIL-101(Fe) could be an ideal candidate to establish such a scenario. To test this hypothesis, the Hep_MIL-101(Fe) composite was introduced into the structure of a boehmite-based thrombolytic sol–gel material. The resulting hybrid material consisting of Hep_MIL-101(Fe) and thrombolytic enzyme streptokinase (SK) entrapped within alumina (designated as Hep_MIL-101(Fe) + SK@alumina) was applied on polytetrafluoroethylene (PTFE) vein implants. The surface coating with a thickness of 300 nm was formed in the course of an irreversible sol–gel transition. Briefly, streptokinase and Hep_MIL-101(Fe) were

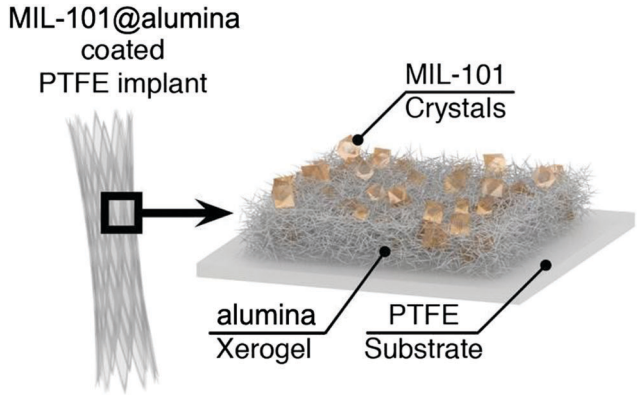

Fig. 6 Visual interpretation of Hep_MIL-101 + SK@alumina-coated PTFE implant and structure of composite surface coating.

mixed with a stable boehmite sol and applied onto the surface of the vein implant. After mixing, the negatively charged composite Hep_MIL-101(Fe) particles and SK molecules electrostatically interact and are covered by the positively charged boehmite NPs (isoelectric point = 10).[24] Subsequently, condensation of boehmite NPs occurred followed by the irreversible sol–gel transition to form a ceramic boehmite sol–gel matrix around the immobilized species. Before the condensation step, the sol–gel hybrid was applied as a nanolayer onto the vascular implant. The resulting hybrid ceramic matrix possesses a developed nano-architecture and a high porosity, with a surface area of 380 $m^2 g^{-1}$ and average pore diameter 6 nm. The enzyme molecules and the heparin-loaded MOF crystals are tightly immobilized by the surrounding inorganic sol–gel matrix to prevent leakage (Fig. 6). The structure of the produced hybrid four component heparine–MOF–alumina–enzyme coating is stable and no component leaching was observed. The release profile of heparin is close to the one observed for the free Hep_MIL-101(Fe) and it depends on the heparin mass fraction in the composite. For the composites with 10, 15 and 20 wt% mass fraction of heparin, release reached 0.8, 2 and 18% after 12 hours of incubation (see the ESI,† Fig. S4).

Analysis of the morphology of the formed coatings by SEM with EDX demonstrated the realization of the organization principles of the hybrid material. As shown in Fig. 7a, a mixture of alumina sol and MOF crystals formed a dense xerogel coating. At a higher magnification, the gel appears uniform with a good distribution of crystals across the volume of the coating. The EDX mapping showed a homogeneous distribution of alumina and MOF components as can be seen from the respective Al- and Fe-Kα signals. Furthermore, the MOF crystals were effectively embedded into the alumina matrix forming a single monolithic layer (Fig. 7b). For the Hep_MIL-101@alumina composite, the multilayer EDX-mapping showed that the crystals inside the structure were observable through the opening in the coating. It is worth noting that the sulfur EDS map showed traces of sulfur (from heparin molecules) distributed in MOF crystals. Despite the small concentration of sulfur in the material that is insufficient to build an EDS map, its signal in the spectrum further confirmed the presence of heparin drug in the hybrid coating composite.

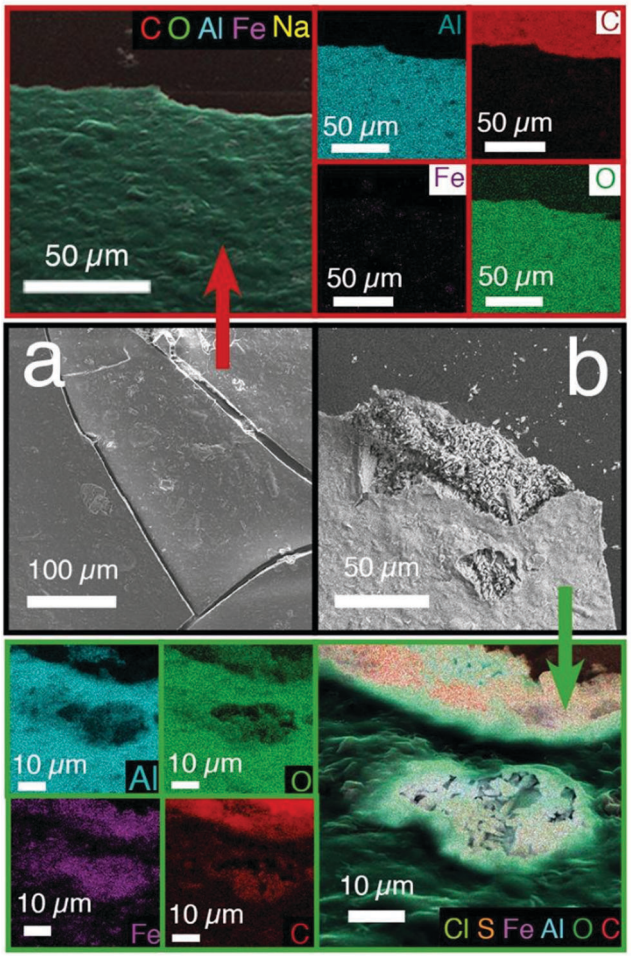

Fig. 7 Microphotographs of the coating (a) and structure of the layer (b) with EDS-mapping of the surface.

Due to the simultaneous presence and uniform distribution of the thrombolytic and anticoagulant agents in one matrix, the hybrid material demonstrated a dual potency in both preventing *de novo* formation of plasma clots and lysing the pre-formed clots. This remarkable bioactivity was demonstrated *in vitro* by measuring the time course of plasma coagulation and clot lysis. The hybrid material was mixed with donor plasma followed by the addition of thrombin (see Experimental section). As shown in Fig. 8, after the addition of thrombin, the optical density of the solution increased within the initial seconds (Fig. 8, brown curve) due to conversion of fibrinogen to fibrin. By 115 s, the clot formation was complete. As expected, free (unbound) heparin potently inhibited coagulation. Likewise, the Hep_MIL-101(Fe) + SK@alumina hybrid also abrogated clot formation (green curve). No detectable clot formation was observed for as long as 800 s after the addition of thrombin and the new material. In contrast, the SK@alumina composite (blue) demonstrated a characteristic kinetic curve with a reversible optical density increase: thrombin addition led to the clot formation process accompanied by a process of clot lysis facilitated by the plasmin-activating SK@alumina composite. The balance between these two opposed processes results in a reversal of the coagulation curve at the 76 s time point.

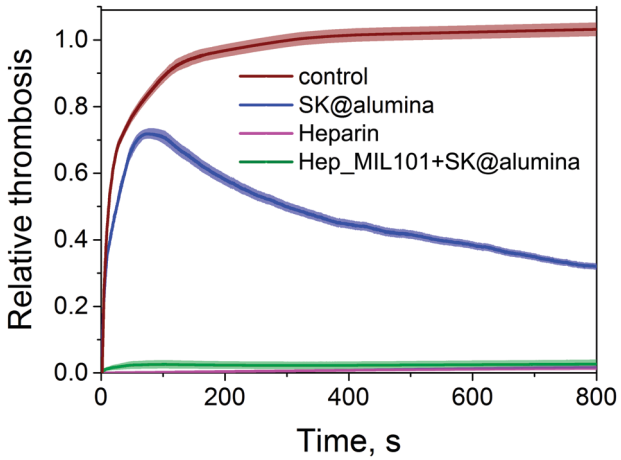

Fig. 8 Time course of plasma clot formation in the presence of heparin (purple), Hep_MIL-101(Fe) + SK@alumina hybrid (green) and and SK@alumina composite (blue). Brown, no drug or material (control).

In these experiments, the concentrations of free and entrapped heparin were equal (100 IU). These data indicated that the Hep_MIL-101(Fe) + SK@alumina composite exhibited similar anticoagulant potency *in vitro* as the reference heparin.

Next, the coating of Hep_MIL-101(Fe) + SK@alumina showed thrombolytic activity similar to that described earlier for sol–gel thrombolytic systems.[35,36] To investigate the ability of the hybrid material to degrade the pre-formed plasma clots, Hep_MIL-101(Fe) + SK@alumina was deployed on glass strrips and the plasma clots were placed on the formed coating with subsequent microscopic monitoring (Fig. 9). The plasma clot on top of the coating decomposed over time (Fig. 9a–c) whereas the control clot on the non-doped alumina coating remained unaltered (Fig. 9d–f). Interestingly, the clot was lysed not only at the periphery but also in its center, strongly suggesting that the coating produces plasmin across its entire surface. According to the images, clot destruction was characterized by its fragmentation, with an increase in the contact area between the surface of the plasmin and fibrin network, which results in faster thrombolysis over time. The hybrid material demonstrated a similar rate of lysis to the SK@alumina thrombolytic coating with complete lysis by 150 min and 134 min, respectively. A slight retardation of clot lysis was apparently due to a decreased area of contact due to the presence of Hep_MIL-101(Fe) crystals on the coating surface.

To demonstrate the efficacy of the hybrid anticoagulant–thrombolytic coating, a test circulating model was applied where standard human plasma was pumped in a circled system by a peristaltic pump. Three different setups were tested: the standard PTFE vein implant, PTFE vein implant coated by SK@alumina thrombolytic coating and PTFE vein implant coated by hybrid Hep_MIL-101(Fe) + SK@alumina hybrid. In order to evaluate the system in a total volume of circulating plasma (20 mL), 0.5 mL of thrombin solution was injected and 1 h later the system was checked for clogging. Dissection of the vein tube demonstrated that injection of thrombin into circulating plasma initiated the fibrin generation and clot formation.

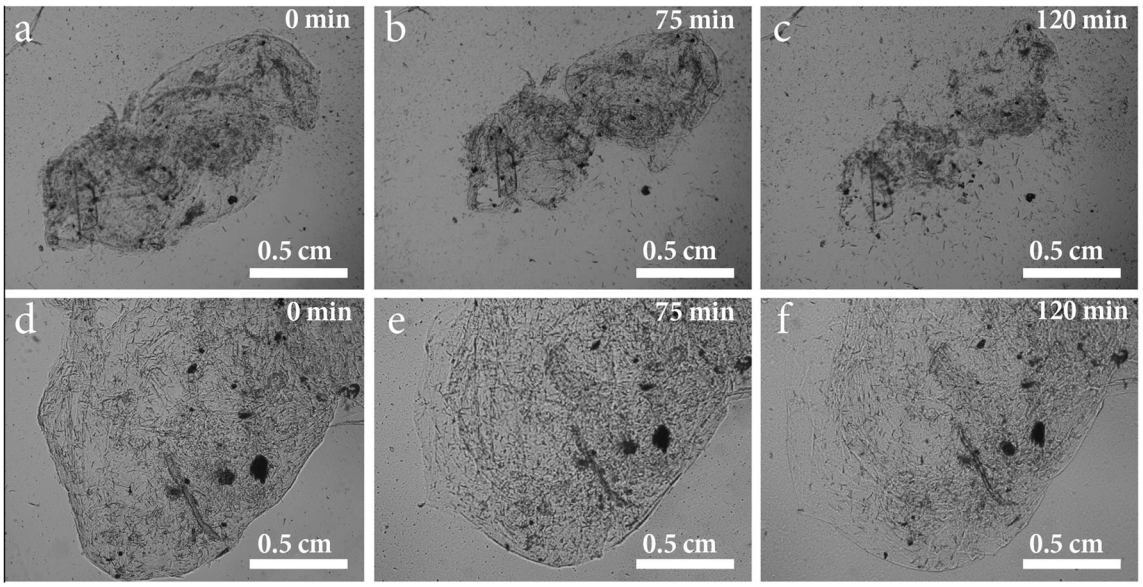

Fig. 9 Plasma clot lysis on alumina sol–gel coatings. Lysis on Hep_MIL-101(Fe) + SK@alumina composite after 0 (a), 75 min (b), and 150 min (c). Control plasma clot on alumina alone after 0 (d), 75 min (e), and 150 min (f).

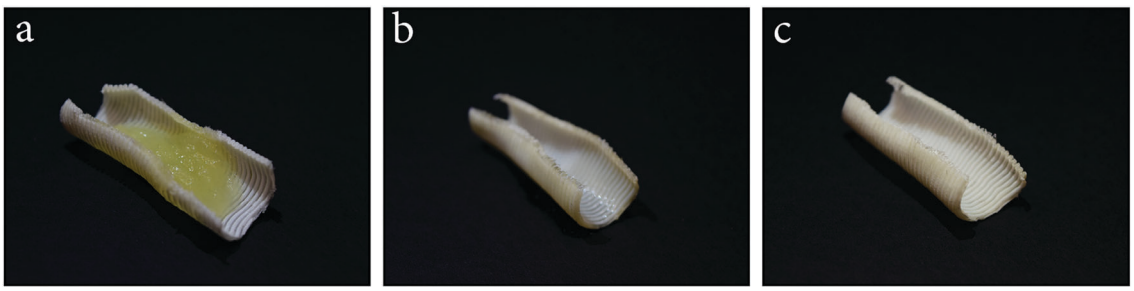

Fig. 10 Coagulation of human plasma in circulating model. The PTFE vein implant untreated (a), coated with SK@alumina (b), or coated with the Hep_MIL-101(Fe) + SK@alumina hybrid (c).

One hour post injection, the plasma circulated in the untreated PTFE vein was fully coagulated (see large clogging in Fig. 10a). In contrast, for the hybrid anticoagulant–thrombolytic coating, no clot formation was observed (Fig. 10c). In full accordance with the results obtained in the cuvette, the hybrid material coating demonstrated the anticoagulant activity strong enough to prevent plasma coagulation in the circulating system. For the thrombolytic SK@alumina coating, evidence of minor local coagulation was observed on the surface of the vein implant, while the majority of the system was liquid. Visual observation showed that 5% of the thrombolytic coating surface was covered by a fibrin layer (Fig. 10b), probably due to nanopore clogging and partial prevention of entrapped SK from implementing its thrombolytic effect. This result proved the concept that the Hep_MIL-101(Fe) composite can be incorporated into the structure of functional nanocomposites and serve as a depot of heparin for anticoagulant activity.

3 Conclusions

In this study, we described the application of a biocompatible MIL-101(Fe) MOF as a carrier for the anticoagulant drug heparin. The iron based MIL-101(Fe) can absorb up to 15 wt% heparin. Adsorption of heparin occurs along with partial decomposition of the MIL-101(Fe) structure, ligand exchange and strong exothermic complexation of heparin sulphate groups with iron atoms in the MIL-101(Fe) lattice. Altogether, this ensures a high heparin adsorption capacity and makes the resulting composite material stable to heparin leakage in aqueous media. The Hep_MIL-101(Fe) composite is negligibly cytotoxic against mammalian cells in concentrations up to 40 μM on a HCT116 cell line, evidencing good biocompatibility and presenting itself as a potential agent for drug delivery applications. In human plasma, Hep_MIL-101(Fe) demonstrates strong anticoagulant activity comparable to free heparin and acts as a heparin depot for prolonged anticoagulant activity. Co-entrapment of the Hep_MIL-101(Fe) crystals into the thrombolytic alumina-based sol–gel coating allowed the bioactivity of the material to be extended and premature clogging of the thrombolytic coating to be prevented.

Conflicts of interest

There are no conflicts to declare.

Acknowledgements

Synthesis and cytotoxicity tests were carried out with the support of Russian Science Foundation, grant no. 16-13-00041. Calculations and modeling were supported by the Ministry of Education and Science of Russian Federation (Project 11.1706.2017/4.6). We would like to thank Leipzig University, the Erasmus+ mobility program, and the Brazilian fellowship program "Science Without Borders" (scholarship for R. P.) for financial support.

References

1 D. Liu, F. Yang, F. Xiong and N. Gu, *Theranostics*, 2016, **6**, 1306.
2 R. M. Sawant, J. Hurley, S. Salmaso, A. Kale, E. Tolcheva, T. Levchenko and V. Torchilin, *Bioconjugate Chem.*, 2006, **17**, 943–949.
3 C. Alvarez-Lorenzo and A. Concheiro, *Chem. Commun.*, 2014, **50**, 7743–7765.
4 S. Mura, J. Nicolas and P. Couvreur, *Nat. Mater.*, 2013, **12**, 991.
5 E. I. Anastasova, V. Ivanovski, A. F. Fakhardo, A. I. Lepeshkin, S. Omar, A. S. Drozdov and V. V. Vinogradov, *Soft Matter*, 2017, **13**, 8651–8660.
6 S. Ganta, H. Devalapally, A. Shahiwala and M. Amiji, *J. Controlled Release*, 2008, **126**, 187–204.
7 B. N. Singh and K. H. Kim, *J. Controlled Release*, 2000, **63**, 235–259.
8 R. H. Müller, K. MaÈder and S. Gohla, *Eur. J. Pharm. Biopharm.*, 2000, **50**, 161–177.
9 M. W. Tibbitt, J. E. Dahlman and R. Langer, *J. Am. Chem. Soc.*, 2016, **138**, 704–717.
10 K. Park, *J. Controlled Release*, 2014, **190**, 3–8.
11 G. Tiwari, R. Tiwari, B. Sriwastawa, L. Bhati, S. Pandey, P. Pandey and S. K. Bannerjee, *Int. J. Pharm. Invest.*, 2012, **2**, 2.
12 P. Horcajada, R. Gref, T. Baati, P. K. Allan, G. Maurin, P. Couvreur, G. Férey, R. E. Morris and C. Serre, *Chem. Rev.*, 2011, **112**, 1232–1268.
13 M. Lismont, L. Dreesen and S. Wuttke, *Adv. Funct. Mater.*, 2017, 27.
14 S. Wuttke, M. Lismont, A. Escudero, B. Rungtaweevoranit and W. J. Parak, *Biomaterials*, 2017, **123**, 172–183.
15 C. He, D. Liu and W. Lin, *Chem. Rev.*, 2015, **115**, 11079–11108.
16 T. Faust, *Nat. Chem.*, 2015, **7**, 270.
17 A. V. Vinogradov, H. Zaake-Hertling, A. S. Drozdov, P. Lönnecke, G. A. Seisenbaeva, V. G. Kessler, V. V. Vinogradov and E. Hey-Hawkins, *Chem. Commun.*, 2015, **51**, 17764–17767.
18 S. Rojas, F. J. Carmona, C. R. Maldonado, P. Horcajada, T. Hidalgo, C. Serre, J. A. Navarro and E. Barea, *Inorg. Chem.*, 2016, **55**, 2650–2663.
19 L.-L. Tan, H. Li, Y.-C. Qiu, D.-X. Chen, X. Wang, R.-Y. Pan, Y. Wang, S. X.-A. Zhang, B. Wang and Y.-W. Yang, *Chem. Sci.*, 2015, **6**, 1640–1644.
20 Z. Tian, X. Yao, K. Ma, X. Niu, J. Grothe, Q. Xu, L. Liu, S. Kaskel and Y. Zhu, *ACS Omega*, 2017, **2**, 1249–1258.
21 M.-X. Wu and Y.-W. Yang, *Adv. Mater.*, 2017, **29**, 1606134.
22 A. Schneemann, V. Bon, I. Schwedler, I. Senkovska, S. Kaskel and R. A. Fischer, *Chem. Soc. Rev.*, 2014, **43**, 6062–6096.
23 Z. Dong, Y. Sun, J. Chu, X. Zhang and H. Deng, *J. Am. Chem. Soc.*, 2017, **139**, 14209–14216.
24 N. Yanai, T. Uemura, M. Inoue, R. Matsuda, T. Fukushima, M. Tsujimoto, S. Isoda and S. Kitagawa, *J. Am. Chem. Soc.*, 2012, **134**, 4501–4504.
25 K. W. Chapman, D. F. Sava, G. J. Halder, P. J. Chupas and T. M. Nenoff, *J. Am. Chem. Soc.*, 2011, **133**, 18583–18585.
26 H. Deng, C. J. Doonan, H. Furukawa, R. B. Ferreira, J. Towne, C. B. Knobler, B. Wang and O. M. Yaghi, *Science*, 2010, **327**, 846–850.
27 W. Kleist, F. Jutz, M. Maciejewski and A. Baiker, *Eur. J. Inorg. Chem.*, 2009, 3552–3561.
28 H. Zheng, Y. Zhang, L. Liu, W. Wan, P. Guo, A. M. NystrÃ¶m and X. Zou, *J. Am. Chem. Soc.*, 2016, **138**, 962–968.
29 J. Kim, H. S. Kim, N. Lee, T. Kim, H. Kim, T. Yu, I. C. Song, W. K. Moon and T. Hyeon, *Angew. Chem., Int. Ed.*, 2008, **47**, 8438–8441.
30 A. S. Drozdov, O. E. Shapovalova, V. Ivanovski, D. Avnir and V. V. Vinogradov, *Chem. Mater.*, 2016, **28**, 2248–2253.
31 P. Saint-Cricq, S. Deshayes, J. Zink and A. Kasko, *Nanoscale*, 2015, **7**, 13168–13172.
32 J. Zhuang, C.-H. Kuo, L.-Y. Chou, D.-Y. Liu, E. Weerapana and C.-K. Tsung, *ACS Nano*, 2014, **8**, 2812–2819.
33 E. M. Shabanova, A. S. Drozdov, V. Ivanovski, I. I. Suvorova and V. V. Vinogradov, *RSC Adv.*, 2016, **6**, 84354–84362.
34 Y. E. Chapurina, A. S. Drozdov, I. Popov, V. V. Vinogradov, I. P. Dudanov and V. V. Vinogradov, *J. Mater. Chem. B*, 2016, **4**, 5921–5928.
35 A. S. Drozdov, V. V. Vinogradov, I. P. Dudanov and V. V. Vinogradov, *Sci. Rep.*, 2016, **6**, 28119.
36 Y. Chapurina, V. V. Vinogradov, A. V. Vinogradov, V. E. Sobolev, I. P. Dudanov and V. V. Vinogradov, *J. Med. Chem.*, 2015, **58**, 6313–6317.
37 E. Bellido, T. Hidalgo, M. V. Lozano, M. Guillevic, R. Simón-Vázquez, M. J. Santander-Ortega, Á. González-Fernández, C. Serre, M. J. Alonso and P. Horcajada, *Adv. Healthcare Mater.*, 2015, **4**, 1246–1257.
38 L. Oar-Arteta, T. Wezendonk, X. Sun, F. Kapteijn and J. Gascon, *Mater. Chem. Front.*, 2017, **1**, 1709–1745.
39 S. M. Rogge, A. Bavykina, J. Hajek, H. Garcia, A. I. Olivos-Suarez, A. Sepúlveda-Escribano, A. Vimont, G. Clet, P. Bazin and F. Kapteijn, *Chem. Soc. Rev.*, 2017, **46**, 3134–3184.
40 A. Dhakshinamoorthy, A. M. Asiri and H. Garcia, *ACS Catal.*, 2017, **7**, 2896–2919.
41 E. A. Pidko, *ACS Catal.*, 2017, 1709–1745.
42 S. DeLauder, F. P. Schwarz, J. C. Williams and D. H. Atha, *Biochim. Biophys. Acta, Protein Struct. Mol. Enzymol.*, 1992, **1159**, 141–149.
43 Y.-H. Hsin, C.-F. Chen, S. Huang, T.-S. Shih, P.-S. Lai and P. J. Chueh, *Toxicol. Lett.*, 2008, **179**, 130–139.
44 X. Yu, R. He, S. Li, B. Cai, L. Zhao, L. Liao, W. Liu, Q. Zeng, H. Wang and S.-S. Guo, *et al.*, *Small*, 2013, **9**, 3895–3901.
45 Y. Lee, H. Lee, Y. B. Kim, J. Kim, T. Hyeon, H. Park, P. B. Messersmith and T. G. Park, *Adv. Mater.*, 2008, **20**, 4154–4157.

46 G. Chatzinikolaou, D. Nikitovic, A. Berdiaki, A. Zafiropoulos, P. Katonis, N. Karamanos and G. Tzanakakis, *Cell Proliferation*, 2010, **43**, 9–18.
47 A. Santiago-Portillo, S. Navaloìn, F. G. Cirujano, F. X. L. I. Xamena, M. Alvaro and H. Garcia, *ACS Catal.*, 2015, **5**, 3216–3224.
48 O. A. Kholdeeva, I. Y. Skobelev, I. D. Ivanchikova, K. A. Kovalenko, V. P. Fedin and A. B. Sorokin, *Catal. Today*, 2014, **238**, 54–61.
49 C. Li, H. Du, A. Yang, S. Jiang, Z. Li, D. Li, J. L. Brash and H. Chen, *Adv. Funct. Mater.*, 2017, **27**, 1703934.
50 A. S. Drozdov, K. V. Volodina, V. V. Vinogradov and V. V. Vinogradov, *RSC Adv.*, 2015, **5**, 82992–82997.